Three-Dimensional Architecture of Grana and Stroma Thylakoids of Higher Plants as Determined by Electron Tomography[1][W][OA]

Jotham R. Austin, II* and L. Andrew Staehelin

Department of Molecular Genetics, and Cell Biology and Advance Electron Microscopy Facility, University of Chicago, Chicago, Illinois 60637 (J.R.A.); and Department of Molecular, Cellular and Developmental Biology, University of Colorado, Boulder, Colorado 80309 (L.A.S.)

We have investigated the three-dimensional (3D) architecture of the thylakoid membranes of Arabidopsis (*Arabidopsis thaliana*), tobacco (*Nicotiana tabacum*), and spinach (*Spinacia oleracea*) with a resolution of approximately 7 nm by electron tomography of high-pressure-frozen/freeze-substituted intact chloroplasts. Higher-plant thylakoids are differentiated into two interconnected and functionally distinct domains, the photosystem II/light-harvesting complex II-enriched stacked grana thylakoids and the photosystem I/ATP synthase-enriched, nonstacked stroma thylakoids. The grana thylakoids are organized in the form of cylindrical stacks and are connected to the stroma thylakoids via tubular junctions. Our data confirm that the stroma thylakoids are wound around the grana stacks in the form of multiple, right-handed helices at an angle of 20° to 25° as postulated by a helical thylakoid model. The junctional connections between the grana and stroma thylakoids all have a slit-like architecture, but their size varies tremendously from approximately 15 × 30 nm to approximately 15 × 435 nm, which is approximately 5 times larger than seen in chemically fixed thylakoids. The variable slit length results in less periodicity in grana/stroma thylakoid organization than proposed in the original helical model. The stroma thylakoids also exhibit considerable architectural variability, which is dependent, in part, on the number and the orientation of adjacent grana stacks to which they are connected. Whereas some stroma thylakoids form solid, sheet-like bridges between adjacent grana, others exhibit a branching geometry with small, more tubular sheet domains also connecting adjacent, parallel stroma thylakoids. We postulate that the tremendous variability in size of the junctional slits may reflect a novel, active role of junctional slits in the regulation of photosynthetic function. In particular, by controlling the size of junctional slits, plants could regulate the flow of ions and membrane molecules between grana and stroma thylakoid membrane domains.

The term thylakoid is the name coined by Menke (1962) to describe the internal photosynthetic membranes of chloroplasts. Most of our knowledge of the three-dimensional (3D) architecture of higher-plant thylakoids is based on the analysis of electron micrographs of thin-sectioned in situ and isolated chloroplasts (Staehelin, 2003). The first electron micrographs of thin-sectioned chloroplasts in which the internal thylakoid membranes were clearly resolved indicated that they were organized in the form of flat sheets and membrane stacks (Hodge et al., 1955; Steinmann and Sjöstrand, 1955). Menke (1960) subsequently postulated that higher-plant chloroplasts contained many individual, sac-like thylakoids of two types, small thylakoids that gave rise to the grana stacks, and large thylakoids (now called stroma thylakoids) that interconnected the grana stacks. Menke's (1960) model was challenged by Weier and coworkers (Weier, 1961; Weier et al., 1963), whose micrographs showed that the stroma thylakoids were not only connected to grana thylakoids, but also formed a tubular network that linked grana thylakoids in adjacent stacks as well as grana thylakoids at different levels in a given stack. Heslop-Harrison (1963) and Wehrmeyer (1964), to our knowledge, were the first to show that the stroma thylakoids were arranged in a spiral-like configuration around grana stacks, and that at each grana-stroma membrane intersection the two membranes were fused together. Their models set the stage for the classic studies of Paolillo and coworkers (Paolillo et al., 1967; Paolillo, 1970), who demonstrated that each grana stack was associated with multiple, parallel spiraling stroma thylakoids (2–12; typically eight), and that the ascending stroma thylakoids always form right-handed helices. One architectural feature highlighted in Paolillo's (1970) model is the amount of 3D connectedness between all thylakoids of a given chloroplast, thus suggesting that all thylakoid lumen form a continuum.

Central predictions of Paolillo's (1970) model such as the helical organization of multiple parallel stroma thylakoids around a given grana stack, and the tubular

[1] This work was supported by the U.S. Department of Agriculture Cooperative State Research, Education, and Extension Service (grant no. 2003–02588 to J.R.A.) and by NIH-NCRR grant P41RR000592.

* Corresponding author; e-mail jotham@uchicago.edu.

The author responsible for distribution of materials integral to the findings presented in this article in accordance with the policy described in the Instructions for Authors (www.plantphysiol.org) is: Jotham R. Austin, II (jotham@uchicago.edu).

[W] The online version of this article contains Web-only data.

[OA] Open Access articles can be viewed online without a subscription.

www.plantphysiol.org/cgi/doi/10.1104/pp.110.170647

connections between the grana thylakoids and adjoining stroma thylakoids have been observed by freeze-fracture electron microscopy (Staehelin and Arntzen, 1983; Staehelin and van der Staay, 1996). The spiral organization of the stroma membranes around mechanically isolated grana stacks has also been visualized by means of scanning electron microscopy (Mustárdy and Jánossy, 1979). Although these freeze-fracture and scanning electron microscopy studies provided interesting new perspectives on the 3D architecture of grana and stroma thylakoids, they did not yield any new insights necessitating major revisions to the Paolillo (1970) model. Thus, the more recently published 3D models of grana and stroma thylakoids (Staehelin and van der Staay, 1996; Mustárdy and Garab, 2003) should be viewed as slightly refined iterations of Paolillo's (1970) thylakoid model rather than new thylakoid models.

An alternative model known as the forked or folded membrane model originated from an attempt to illustrate in a simple diagram how PSI and PSII are segregated into stroma and grana membrane domains (Andersson and Anderson, 1980; Anderson and Andersson, 1988). More recently, a computerized version of this model was developed (Arvidsson and Sundby, 1999) to explain the rapid, cation-induced changes in chlorophyll-a fluorescence (Briantais, 1984), which have been postulated to reflect changes in membrane architecture related to unstacking and restacking of the thlakoid membranes. To date, no ultrastructural studies have been published in support of the forked/folded membrane model except for some of the data presented in the recent electron tomography article of Shimoni et al. (2005), which are discussed in greater detail below.

Due to the approximately 20-fold-higher *z* axis resolution of electron tomography (6–8 nm) compared to serial thin-section electron microscopy (120–160 nm; McIntosh et al., 2005; Donohoe et al., 2006), electron tomography has the potential of yielding novel information on the 3D structure of thylakoids. Three electron tomography studies of higher-plant thylakoids have been published to date (Shimoni et al., 2005; Mustárdy et al., 2008; Daum et al., 2010). Unexpectedly, the first of these investigations (Shimoni et al., 2005) yielded a thylakoid model that differed from the Paolillo (1970) model, whereas the data presented in the two latter studies (Mustárdy et al., 2008; Daum et al., 2010) appear to support the model.

Shimoni et al. (2005) investigated the structure of thylakoids in intact chloroplasts of high-pressure-frozen/freeze-substituted lettuce (*Lactuca sativa*) leaf cells. Although the chloroplasts appear well frozen, the heavy staining of the chloroplast stroma and the resulting negative staining of the thylakoid membranes limit the overall resolution of the samples. In turn, the lack of positive staining of the membranes also makes it more difficult to produce precise tracings of the membranes for model building. Nevertheless, the authors state that their tomograms provide support for a novel thylakoid model that contains elements of the folded membrane model (Anderson and Andersson, 1988). The novel thylakoid model of Shimoni et al. (2005) is described as follows by the authors: "The granum layers are formed by bifurcation and subsequent fusion of the membranes rather than by invagination or folding. Adjacent layers in the granum are not connected to each other through the stroma lamellae. Instead, they are interconnected directly through their edges, which bend toward and fuse with neighboring layers" (p. 2583). Unfortunately, the limited depth of the tomographic reconstructions reproduced, combined with the poor thylakoid membrane staining, raises questions about the validity of the interpretation of the data that support the postulated novel type of bifurcated grana-stroma thylakoid model.

The electron tomographic data sets of Mustárdy et al. (2008) illustrate isolated spinach (*Spinacia oleracea*) thylakoids chemically fixed with glutaraldehyde and OsO_4 prior to embedding in Spurr's resin. The positively stained membranes are clearly seen against the unstained background of the buffer solution, and the tomographic slice images appear consistent with the Paolillo (1970) model. However, the article lacks a 3D model of reconstructed grana and stroma thylakoids. Furthermore, due to the use of isolated thylakoid membranes that were subjected to mechanical and chemical stresses during the thylakoid isolation and chemical fixation processes, it is unclear how accurately the tomographic images reflect the structure of the native membranes. The section of the Daum et al. (2010) article devoted to the 3D architecture of the thylakoid membranes is based on the electron tomography analysis of vitreous, frozen sections of spinach chloroplasts. Due to technical limitations, the reconstructed thylakoid volumes were limited to the thickness of the vitreous sections (approximately 150 nm). However, the 3D models demonstrate a staggered arrangement of the connections between the stroma thylakoids and the grana margins as predicted by the Paolillo (1970) model.

The goal of this study was to produce electron tomography-based models of entire grana stacks and of complete sets of stroma thylakoids between grana stacks in intact chloroplasts preserved by high-pressure-freezing/freeze-substitution methods. To achieve this objective, we also developed a freeze-substitution protocol that enabled us to overcome the problem of negative membrane staining encountered in the Shimoni et al. (2005) investigation. Our 3D thylakoid models based on the tracing of hundreds of approximately 2-nm-thick slice images of serial thick sections are in general agreement with the thylakoid model of Paolillo (1970). However, they have also led to the discovery of characteristic irregularities in the organization of the connecting regions of the spiraling stroma thylakoids with the membranes of the grana stacks, and provide information on the architectural variability of the stroma thylakoids between adjacent grana stacks.

RESULTS

This study reports on an electron tomography study of the 3D architecture of grana and stroma thylakoids of in vivo chloroplasts of tobacco (*Nicotiana tobacum*) and Arabidopsis (*Arabidopsis thaliana*) and of isolated intact spinach chloroplasts (which we found could be used interchangeably) preserved by high-pressure-freezing/freeze-substitution methods. The investigation included the recording of 20 tomograms, the analysis of approximately 4,500 tomographic slice images, and the examination of approximately 300 thin-section electron micrographs. The sections used for the preparation of the tomograms were either 250- or 300-nm thick, and for the reconstruction of larger chloroplast volumes containing multiple grana stacks and associated stroma thylakoids we produced montages consisting of up to 10 individual tomograms (Austin et al., 2005). As detailed below, the resulting thylakoid models both confirm the central elements of the helical grana-stroma thylakoid model of Paolillo (1970), while also revealing architectural details not previously reported.

Stroma Thylakoids Form Multiple, Parallel Helices around the Cylindrical Grana Stacks to Which They Are Connected

The type and quality of the tomographic slice images produced during this investigation is documented in Figure 1 and shown in Supplemental Movie S1. Of particular importance for this study are the positive staining of the grana and stroma thylakoid membranes, the lack of staining of the clearly delineated thylakoid lumen, and the lightly stained stroma in which individual ribosomes and other molecules are readily discerned. Figure 2 illustrates the size of the largest tomographic thylakoid reconstruction produced during the course of this study, which has a volume of approximately $4 \times 4 \times 1.5$ μm (produced from five serial sections, two adjacent x/y axis tomograms per section). Three examples of tomographic slice images used for the reconstruction are illustrated in Figure 2, A to C. The modeled chloroplast volume included three grana stacks of different sizes (yellow), and associated stroma thylakoids (green). However, to better illustrate the different types of stroma thylakoid configurations and grana-stroma thylakoid interactions, we have omitted several of the stroma thylakoids from the model (Fig. 2, D and E).

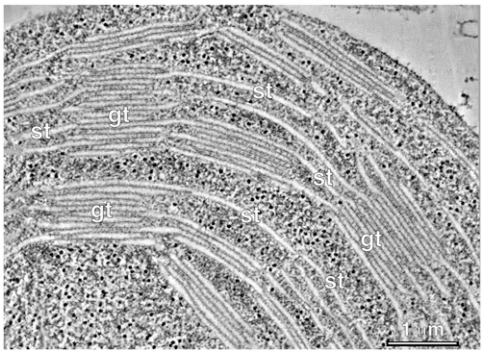

Figure 1. Electron tomogram of a high-pressure-frozen and freeze-substituted chloroplast. Shown is a composite tomographic slice image (five superimposed serial 2.2-nm optical slices) of the interconnecting grana stacked thylakoids (gt) and stroma thylakoids (st).

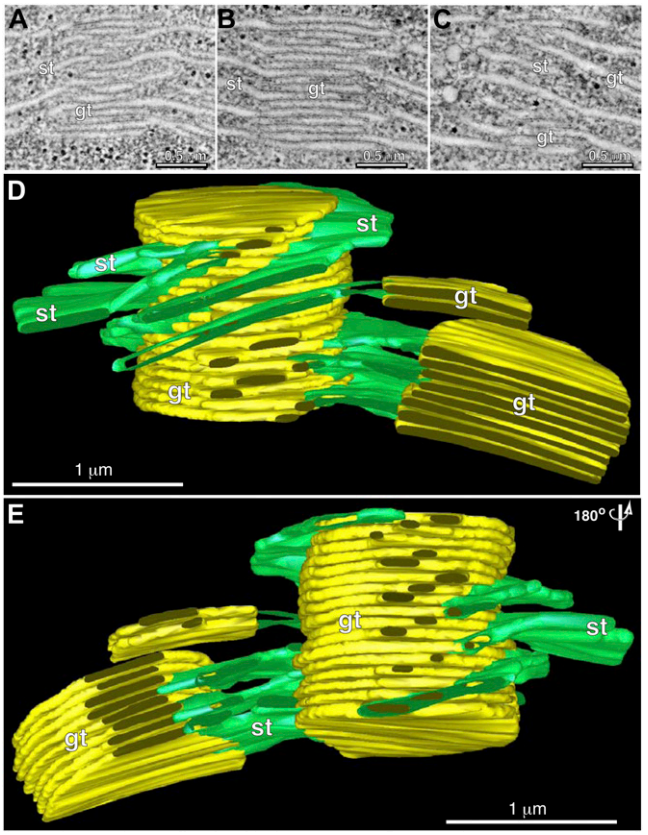

Figure 2. An overview of grana and stroma thylakoid organization. A to C are three composite tomographic slice images (five superimposed 2.2-nm optical slices) showing views from the front (A), middle (B), and back (C) of a grana thylakoid stack. D and E are tomographic reconstructed models of the grana stack shown in A to C, with the grana thylakoids colored yellow and the stroma thylakoids colored green. Front view in D, and the model (E) is rotated 180° to show the back view. Note that for illustrative purposes the model does not display all of the thylakoids associated with the grana stacks.

The models of the cylindrical grana stack and associated stroma thylakoids shown in Figure 3, A and L, are based on approximately 350 serial tomographic slice images, 10 of which are shown in Figure 3, B to K. To help the viewer follow the changes in architecture of individual thylakoids in the different tomographic slice images, as well as correlate the microscopic image data with the structures depicted in the reconstructed thylakoid models, we have labeled the individual stroma thylakoids with different colors and numbers, and the yellow grana thylakoids with letters. Note, for

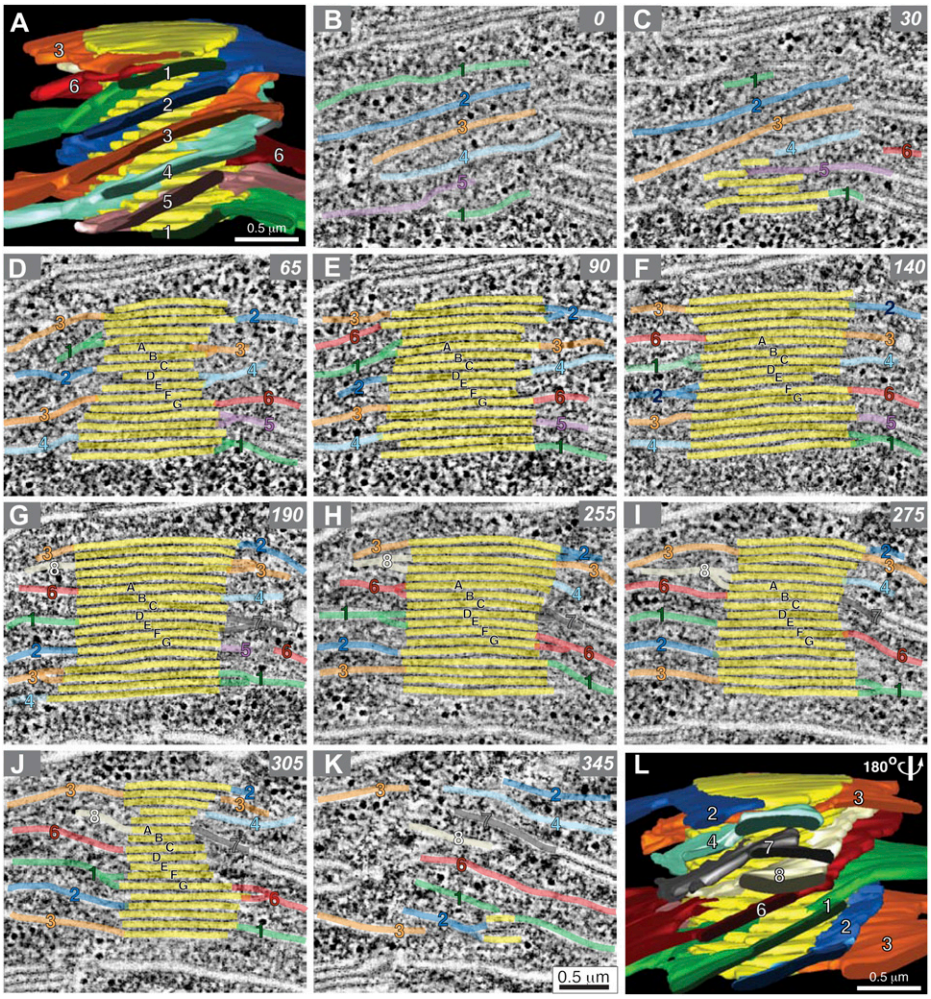

Figure 3. Serial tomographic slice images through a grana thylakoid stack and reconstructed models of the stack. A is a tomographic model of a grana stack. Grana thylakoids are colored yellow, and interconnecting stoma thylakoids are colored and numbered so their position can be tracked in the serial tomographic slices B to K. B to K show serial 2.2-nm tomographic slice images at specific z intervals through the grana stack.

example, that due to its helical geometry, the green stroma thylakoid 1 is seen close to the top of the grana stack as well as near the bottom of the stack in the front-side view of the model (Fig. 3A), and in a diagonal orientation in the bottom half of the back-side view of the model (Fig. 3L). A total of eight stroma thylakoids are wrapped around the grana stack shown in Figure 3. As predicted by the Paolillo (1970) model, the sheet-like stroma thylakoids associated with the stack (Fig. 3, A and L) appear evenly spaced as they spiral up and around the grana stack.

The Junctional Connections between Stroma and Grana Thylakoids Have a Slit-Like Geometry and Are of Variable Size

To characterize the junctional connections between individual spiraling stroma thylakoids and associated grana thylakoids within a stack, we have performed detailed analyses of serial tomographic slice images of the junctions (Fig. 4). The image series starts (Fig. 4A, slice 0) with a slice in which a stroma thylakoid (highlighted in green) is seen to be continuous with the grana thylakoid (yellow) labeled C (arrow). The next image (Fig. 4B, slice 10; 22 nm below) shows the beginning of a membrane branch that links the stroma thylakoid to both grana thylakoid C and grana thylakoid B. A gradual change in geometry of the junctional connection is seen as the slice level progresses to slice 20 (Fig. 4C) and slice 30 (Fig. 4D). In slice 40, the stroma thylakoid appears only connected to grana thylakoid B (Fig. 4E, arrow), and the same type of spatial relationship to grana thylakoid B continues on through slice 60 (Fig. 4F) for a total change in depth of 44 nm. The onset of the next branching point is depicted in slice 70 (Fig. 4G), where the stroma thylakoid again appears connected to two adjacent grana thylakoids (Fig. 4, A and B, arrows). This branching configuration continues through slices 80 and 90 (Fig. 4, H and I). In slice 100 (Fig. 4J) the stroma thylakoid appears only connected to grana thylakoid A. Together these images provide clear evidence for a slit-like architecture of the junctional connections between grana and stroma thylakoids, as well as for the helical configuration (tilt angle 20°–25°) of the stroma thylakoids that spiral up and around the stack (Figs. 2–6). The size of the typical

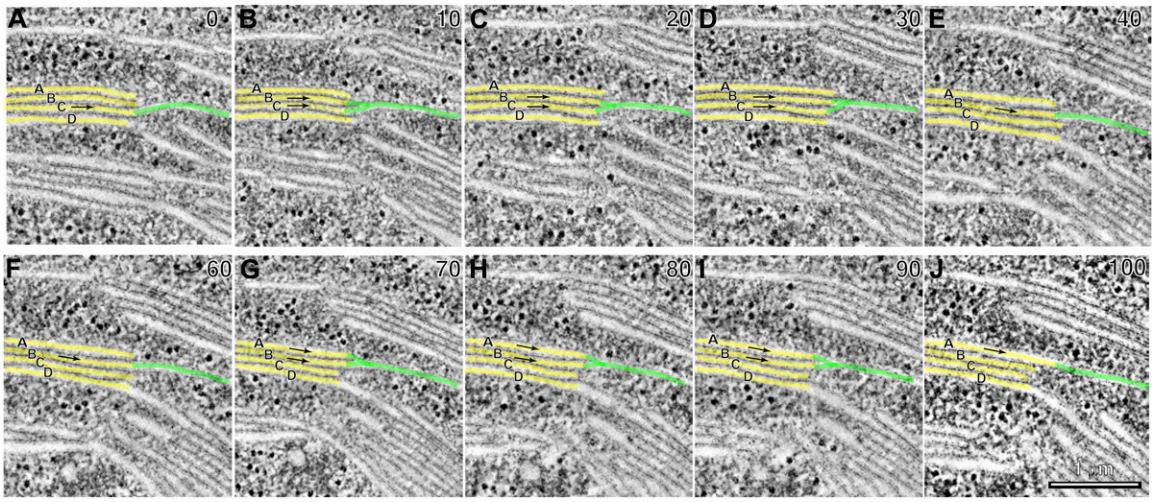

Figure 4. Electron tomogram serial sections illustrating the structure of the junctional connections between grana thylakoids and a helical stroma thylakoid. A to J show serial 2.2-nm tomographic slice images through grana-stroma thylakoid connections. The grana stack thylakoids are colored yellow and lettered A to D, and the stoma thylakoids are colored green. Also, the stroma-grana connections are marked with arrows. Note that in A the stroma thylakoid connects with the grana thylakoid marked C. In B to D the stroma thylakoid connect with grana thylakoids C and B. In E and F the stroma thylakoid is connected with grana thylakoid B only. In G to I the stroma thylakoid is connected with grana thylakoids B and A. Finally in J the stroma thylakoid is connected to grana A only.

junctional slits varies from approximately 15 × 30 nm to approximately 15 × 435 nm (Fig. 7). Upon closer examination of the histogram of slit lengths, it is seen that the majority of the slits have a length of 30 to 130 nm, and a small number are of the larger type, 150 to 435 nm in length. The spatial relationship between smaller and larger slits on grana stacks is documented in Figures 5 and 6.

A different view of the spiraling architecture of a stroma thylakoid connected to a series of stacked grana thylakoids is presented in Figure 5, A to C. To obtain the tangential-type view of the stroma thylakoid with clear connections (arrows) to seven adjacent, stacked grana thylakoids, we used the slicer tool of the 3dmod modeling program to orient the slice depicted in Figure 5B to match the plane of the spirally organized connecting regions between the stroma thylakoid and the adjacent grana thylakoids. A model of this association is shown in Figure 5D. Interestingly, when this model is analyzed in greater detail, not all of the grana-stroma thylakoid junctional connections are seen to be precisely arranged in a spiral-like configuration, and one of the junctional connections is seen to have twice the slit length (approximately 248 nm) of the others (Fig. 5D, white arrowheads). Another example of a long junctional slit (approximately 307 nm) and the associated interruption of the helical organization of a stroma thylakoid are illustrated in Figure 6 (white arrowheads). As seen most clearly in Figure 6, B and D, the stroma thylakoid adjacent to the grana thylakoid with the longer-length slit also becomes parallel to that grana thylakoid, breaking the helical organization of the stroma thylakoid.

The Architecture of Stroma Thylakoids Connecting Adjacent Grana Stacks Is Variable

Figure 8 depicts tomography-based models of two pairs of grana stacks (yellow) and their interconnecting stroma thylakoids (multiple colors), which illustrate the variable architecture of stroma thylakoids in chloroplasts. The first model (Fig. 8, A–D) shows three parallel, sheet-like stroma thylakoids that form bridging structures between the two grana stacks, but lack any connections to each other. In contrast, the second model (Fig. 8, E–G) displays four spiraling and branching stroma thylakoids that not only bridge the space between the grana stacks, but also form a 3D membrane network that connects grana thylakoids at different levels within each grana stack. To better illustrate the geometry of the connecting regions between the differently colored, but physically continuous stroma thylakoid membrane domains, we only show the green (semitransparent) and the red stroma thylakoids in the tilted model image Figure 8F, and the red and blue stroma thylakoids in Figure 8G.

DISCUSSION

The goal of this study was to produce a detailed understanding of the 3D architecture of higher-plant thylakoids by means of electron tomography analysis of high-pressure-frozen/freeze-substituted in situ and in vitro chloroplasts. Our results confirm central features of the helical thylakoid model of Paolillo (1970) and have added novel insights into the variability of

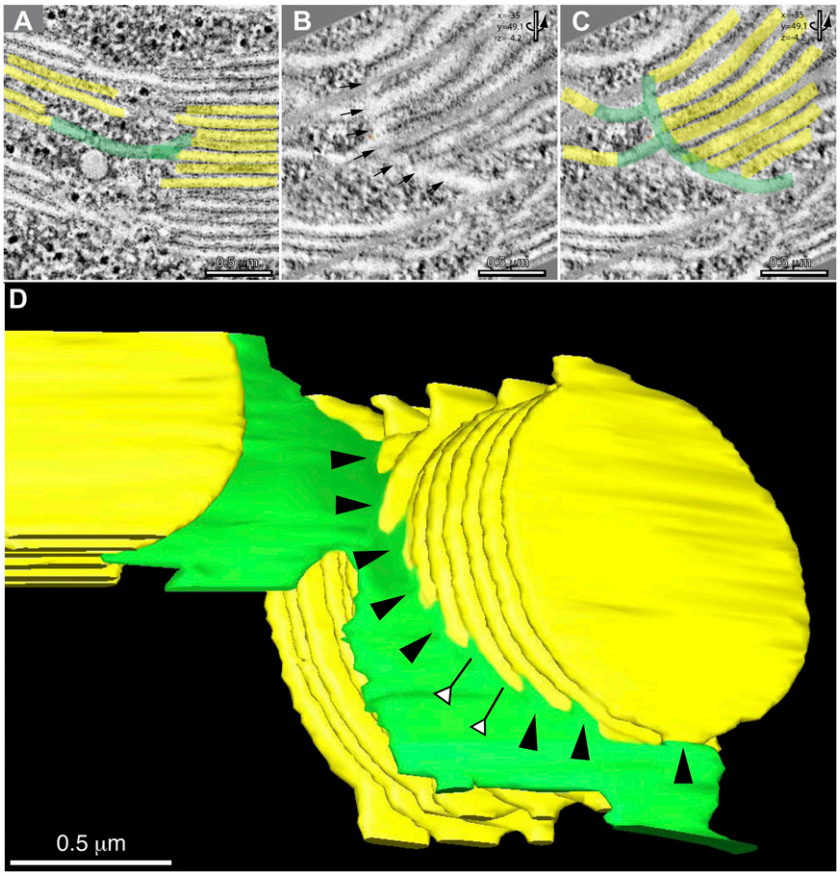

Figure 5. Tomographic model of a granum with associated stroma thylakoid. A depicts an image composed of five superimposed 2.2-nm serial tomographic slices. Grana thylakoids are colored yellow with interconnected stroma thylakoids colored green. B, Rotated ($x = -35$, $y = 49.1$, and $z = -4.23$) tomographic slice image of A. Note the stroma thylakoid connects with seven grana thylakoid membranes (marked with arrows). C is a colored version of B, with grana thylakoids highlighted yellow and stroma thylakoids green. D shows a tomographic model of the grana stack and stoma thylakoid shown in A. The black arrowheads mark the smaller-size, slit-like stroma-grana connections, whereas the white arrowheads mark one stroma-grana connection that is approximately twice the length of the other stroma-grana connections. See histogram Figure 7 for quantitative information on the slit size dimensions.

junctional slit sizes and the architecture of stroma thylakoids (summarized in the 3D model in Supplemental Fig. S1), but are inconsistent with the predictions of the forked or folded membrane model of Andersson and Anderson (1980) and Arvidsson and Sundby (1999) and with the electron tomography-based bifurcated thylakoid model of Shimoni et al. (2005).

Membrane Stacking Is a Common Feature of Bacterial, Algal, and Higher-Plant Photosynthetic Membranes

The differentiation of thylakoid membranes into stacked and nonstacked membrane domains has a long evolutionary history (Staehelin, 1986). For example, the nonoxygen evolving, purple photosynthetic bacterium *Rhodopseudomonas palustris* contains large stacks of thylakoid membranes (Varga and Staehelin, 1983) as does the oxygen-evolving cyanobacterium *Prochloron* (Giddings et al., 1980), which lacks phycobilisomes but contains a chlorophyll *a*/*b* pigment protein complex that resembles light-harvesting complex II (LHCII), the main membrane adhesion factor of higher-plant thylakoids (McDonnel and Staehelin, 1980). Similar stacked thylakoid membrane domains capable of segregating different types of protein complexes into different membrane domains are characteristic features of green algae such as *Chlamydomonas reihardtii* (Goodenough and Staehelin, 1971) and *Euglena gracilis* (Miller and Staehelin, 1973). In higher plants, the stacked membrane domain architecture has evolved into structures known as grana stacks (Menke, 1962).

The development of laterally differentiated stacked (grana) and nonstacked (stroma) thylakoid membranes appears to have conveyed several evolutionary advantages to photosynthetic organisms carrying these traits. One major advantage relates to the fact that the formation of grana stacks enables plants to package large expanses of photosynthetically active thylakoid membranes into the relatively small volume of chloroplasts. The formation of stacked membrane domains also provides a means for fine tuning of photosynthethic functions such as optimizing the rates of turnover of PSI and PSII, and the flow of electron through the electron transport chain (Staehelin and Arntzen, 1983; Trissl and Wilhelm, 1993; Anderson, 1999; Kirchhoff et al., 2007). In addition, grana allow for the incorporation of large light-harvesting antennae for PSII into the thylakoid membranes without excessively restricting electron transport (Mullineaux, 2005). The ratio of grana to stroma membrane domains in higher-plant chloroplasts is highly variable, with low-light plants of rain forests such as *Alocasia macrorhiza* producing much larger, up to 100 grana thylakoid-containing stacks (Anderson et al., 1973), than high-light plants grown in full sunlight (5–15 grana thylakoids).

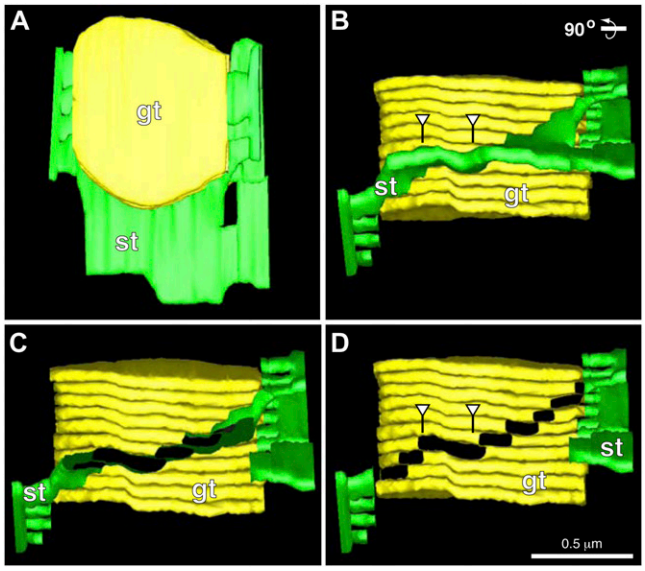

Figure 6. Spatial distribution of differently sized grana-stroma connections on a grana stack. A is a tomographic model showing the top view of a grana stack (gt), with interconnected stroma thylakoids (st). B is a rotated (90°) tomographic model of A. C is a tomographic model of B where the stroma thylakoid has been partially cut away to reveal the connection site between the stroma and grana membranes (highlighted black). D is a tomographic model in which all of the stroma thylakoid membrane on the front side of the grana stack have been removed, revealing all of the stroma-grana connecting sites (highlighted in black). Note the white arrowheads pointing to a stroma-grana connecting site that is much longer than the others.

Stroma Thylakoids Wind around Grana Stacks in a Helical Fashion and Are Connected to the Grana Thylakoids via Slits in the Grana Margins

To take full advantage of the 3D resolution of electron tomography, we have studied exclusively intact chloroplasts preserved by high-pressure-freezing/freeze-substitution methods (Kiss and Staehelin, 1995). The improved structural preservation of thylakoids prepared in this manner compared to chemically fixed and dehydrated samples relates to the fact that freezing allows for all of the molecules within a cell to be immobilized within less than 1 ms (Gilkey and Staehelin, 1986), and that during freeze substitution the frozen water molecules are replaced by acetone while the sample is maintained at −80°C. By optimizing the freeze-substitution and staining protocols we have also produced positive staining of the thylakoid membranes and thereby increased our ability to precisely trace the membranes in our tomographic slice images (Fig. 1). Compared to the thylakoid models derived from serial thin-section reconstructions (Paolillo, 1970; Brangeon and Mustárdy, 1979) the electron tomography models produced during the course of this study have an approximately 20-fold-higher z axis resolution and a slightly increased x/y axis resolution, yielding thylakoid models with a 3D resolution of 6 to 8 nm. Together with the relatively large size of the reconstructed chloroplast volumes (approximately $4 \times 4 \times 1.5$ μm), these data have enabled us to generate high-resolution reconstructions of entire grana stacks and of stroma thylakoids that bridge the space between adjacent stacks (see Supplemental Movie S1).

One of the striking features of our new models is the extent to which they confirm the basic elements of the helical thylakoid model of Paolillo (1970). However, considering the many different types of electron microscope studies that have provided experimental support for this model during the past 40 years (for review, see Mustárdy and Garab, 2003), this result is not unexpected. Most clearly seen in our models is the arrangement of the parallel stroma thylakoids that spiral around the grana stacks as right-handed helices (Figs. 2–6, 8, and Supplemental Figure S1). This helical geometry contradicts central structural predictions of the forked/folded thylakoid membrane model (Andersson and Anderson, 1980; Arvidsson and Sundby, 1999) as well as the bifurcation model of Shimoni et al. (2005).

One of the novel features of our models pertains to the actual geometry of the stroma thylakoids between adjacent grana stacks (Figs. 2, 5, 8, and Supplemental Figure S1). In particular, we demonstrate that where the stroma thylakoids connect to grana thylakoids in adjacent grana stacks that are appropriately tilted with respect to each other, the thylakoids form flat, sheet-like structures (Fig. 5). In contrast, where the parallel helical stroma thylakoid membranes are connected both to adjacent grana stacks and to each other through bridging domains, which also form links between different grana thylakoids within a given grana stack, the stroma thylakoids are branched and exhibit a less-expansive, sheet-like, or even tubular geometry (Fig. 8, E–G).

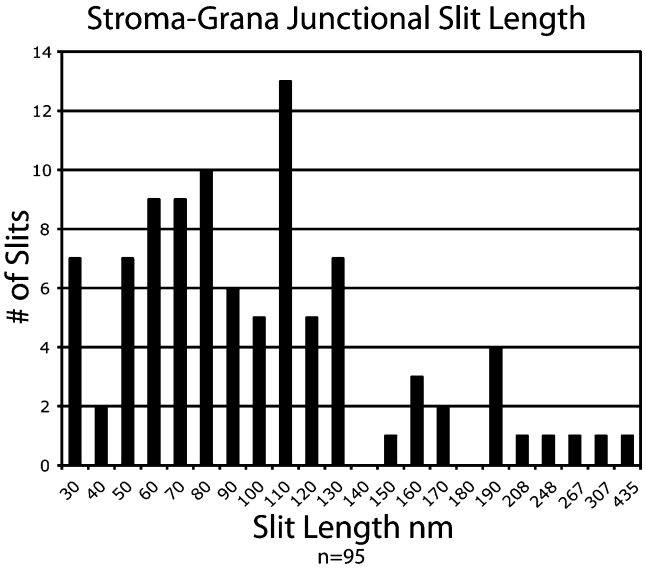

Figure 7. Histogram demonstrating the variation in junctional slit lengths between grana and stroma thylakoids.

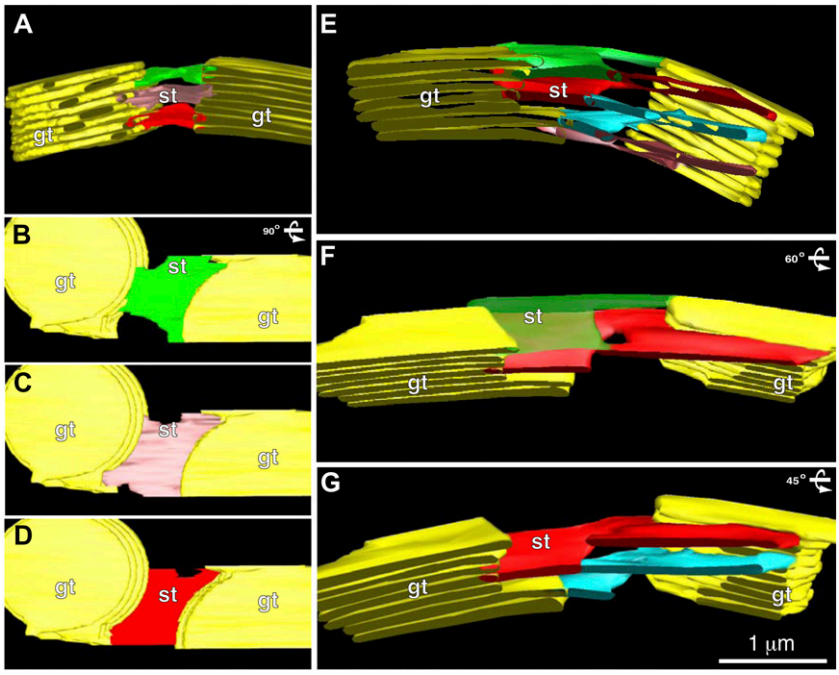

Figure 8. Tomographic models showing the variation in stroma architecture. A shows a tomographic model with parallel, sheet-like stroma thylakoid membranes (st; colored green, pink, and red) that bridge the space between two grana thylakoid stacks (gt; colored yellow), but that are not connected to each other. B to D is the same model as A, but rotated 90° showing the sheet-like architecture of the individual stroma thylakoids; green (B), pink (C), and red (D) stroma thylakoids. E illustrates another tomographic model in which quasi-helical stroma thylakoids (st; colored green, red, turquoise, and pink) are seen to connect two grana stacks (gt; colored yellow). F and G, Same model as E, but F is rotated 60° to better demonstrate the 3D interconnectivity of the green (semitransparent) and the red stroma thylakoid membranes; G is rotated 45° and shows the interconnectivity between the red and turquoise stroma thylakoid membranes.

Another refinement of the helical model necessitated by our data includes a greater amount of variability in the periodicity of the organization of the stroma thylakoids around the grana stacks than previously thought (Figs. 5–7 and Supplemental Fig. S1). As shown in Figure 7, the junctional slits seen in our high-pressure-frozen chloroplasts were not only greater but also more variable in size (30–435 nm) than those reported for the chemically fixed isolated thylakoids (13–70 nm) used in the electron tomography study by Mustardy et al. (2008). The difference in slit size observed in the two studies is most likely due to the use of isolated thylakoids and of chemical fixation methods in the Mustardy et al. (2008) investigation. We do not know what the suspension of isolated thylakoids in a buffer solution does to slit size, but we do know that chemical fixation typically leads to specimen shrinkage (Gilkey and Staehelin, 1986). Also, in the study by Daum et al. (2010), which used cryopreservation and cryo-electron microscopy methods, the junctional slits were reported to be larger than those seen in the Mustárdy et al. (2008) study.

The Variable Size of Junctional Slits Suggests That They May Participate in the Functional Regulation of Thylakoid Activities

The grana-stroma thylakoid membrane system is unique in its 3D complexity, and based on the helical thylakoid model Paolillo (1970), which our data confirmed, it is typically portrayed as a fairly rigid, stable, and inflexible membrane platform. Nevertheless, continuing efforts are being made to explain the regulation of many of the dynamic processes of photosynthesis in the context of changes in thylakoid ultrastructure. Of these, the explanation of state I/II transitions in the context of lateral movements of LHCII proteins and changes in the amount of membrane stacking is best known (Staehelin and Arntzen, 1983; Allen, 1992). However, other thylakoid structure-related regulatory mechanisms may exist that have yet to be identified. Based on the unexpectedly large variations in junctional slit size observed in this study (Fig. 7 and Supplemental Fig. S1), and the ability of these slits to shrink dramatically when exposed to chemical fixatives such as glutaraldhyde, we propose that junctional slit size may be controlled by plants to regulate the movement of protons and of membrane proteins between grana and stroma thylakoid membranes. For example, activation of the kinases that phosphorylate LHCII during state I → II transitions may also induce an increase in slits size to expedite the transfer of the phosphorylated LHCII complexes from grana to stroma thylakoid regions. Similarly, photoinhibitory light conditions might stimulate slit enlargement to facilitate the transfer of damaged PSII complexes to stroma thylakoids for repair (Aro et al., 2004). Yet other regulatory mechanisms might exist that have not been discovered. Alternatively, the differences in slit dimensions may be related to the mechanism of grana thylakoid assembly.

Unstacking of Grana Thylakoids during State I → II Transitions Differs from Unstacking of Isolated Thylakoids in Low-Salt Solutions

There is much confusion in the literature about how the thylakoids of higher plants can become unstacked in low-salt solutions, and how the amount of thylakoid

stacking is reduced during state I → II transitions, considering the complex 3D architecture of the in situ membranes that has been confirmed by this study. The differentiation of thylakoids into stacked grana and nonstacked stroma regions is a reflection of the compositional and functional differences of these membrane domains (Andersson and Anderson, 1980; Staehelin and van der Staay, 1996). Typically, approximately 85% of the PSII and 70% to 90% of the LHCII complexes are confined to grana membranes, and >85% of the PSI and 100% of the ATP synthase complexes are associated with the stroma membranes. The principal thylakoid membrane adhesion factor is LHCII (McDonnel and Staehelin, 1980). In the chlorophyll *b*-less *clorina-f2* mutant of barley (*Hordeum vulgare*) that lacks LHCII the PSII-associated light-harvesting protein Lhcb5 appears to be responsible for stacking, but this stacking requires much higher concentrations of magnesium than LHCII-mediated stacking (Bassi et al., 1985; Król et al., 1995).

Isolated thylakoids can be experimentally unstacked by transfer to zwitterionic buffers of low ionic strength, and restacked by the addition of >3 mM $MgCl_2$ or >150 mM NaCl (Izawa and Good, 1966; Staehelin, 1976). These salt effects can best be explained by neutralization of the negatively charged groups on the LHCII molecules that mediate the intermembrane protein-protein interactions by the cations (Barber, 1982; Dekker and Boekema, 2005). Detailed studies of the changes in thylakoid membrane architecture induced by the different cation concentrations have led to the following findings. Experimental unstacking of higher-plant thylakoids involves three steps (Staehelin, 1986). Stage 1: Rapid (5–10 min when the membranes are kept at 4°C) separation of the appressed membrane regions with minimal changes in the lateral distribution of ATP synthase complexes (Miller and Staehelin, 1976) and PSII complexes (Staehelin et al., 1977). When such membranes are immediately restacked by the addition of cations, the resulting reconstituted grana stacks are nearly indistinguishable for those of control thylakoids. Stage 2: Enlargement of the junctional slits between the grana and stroma thylakoids (15–30 min) dramatically increases the lateral movement and intermixing of the different types of integral protein complexes and bilayer lipids, and results in membrane unfolding via membrane flow (Staehelin et al., 1977). Stage 3: Complete unfolding of the complex 3D thylakoid networks (>30 min) by means of membrane flow that results in complete intermixing of all protein complexes and in the formation of large, interconnected thylakoid membrane sheets (Staehelin, 1976; Staehelin et al., 1977). Addition of cations to stage 3 type unstacked and unfolded thylakoid membranes leads to the reestablishment of large stacked membrane domains (percent stacking equivalent to control membranes) and to a complete reseggregation of all of the protein complexes (Staehelin, 1976). However, these stacked membrane domains are not organized in the form of grana stacks. Recently, it has also been shown that in terms of macromolecular PSII arrangement as well as antenna organization the restacked thylakoid domains are virtually identical to stacked control membranes (Kirchhoff et al., 2007). All of these studies contradict claims made in an earlier study of chemically fixed thylakoid samples that low-salt-induced thylakoid unstacking involves membrane rupturing (Brangeon, 1974), or requires a forked/folded membrane type of grana architecture (Arvidsson and Sundby, 1999).

Because state I/II transitions also induce changes in the amount of thylakoid stacking, many researchers have attempted to explain the state I/II changes in membrane architecture in terms of the cation concentration-dependent changes in thylakoid organization. This analogy has led to wrong conclusions about the changes in thylakoid architecture that accompany state I/II changes and to confusing statements about these changes in the literature.

The term state I/II transition refers to a mechanism employed by algae and higher plants to regulate excitation energy distribution between PSI and PSII (Allen, 1992). This regulation involves the reversible phosphorylation of LHCII by a membrane-bound protein kinase. LHCII phosphorylation reduces the adhesion between LHCII complexes in adjacent thylakoid membranes due to electrostatic repulsion and associated protein conformational changes, and enables the LHCII complexes to separate from the PSII complexes and to migrate laterally though the junctional slits into the PSI-enriched nonstacked stroma thylakoid domains (Staehelin and Arntzen, 1983). Using freeze-fracture electron microscopy to determine the accompanying changes in membrane stacking and distribution of the approximately 8 nm in diameter LHCII complexes between stacked and nonstacked membrane domains, Kyle et al. (1983) have produced quantitative information on state I-state II-induced membrane changes. Thus, using thylakoids isolated from peas (*Pisum sativum*), they observed that between 20% and 25% of the grana LHCII complexes migrated into the stroma thylakoid regions in response to phosphorylation, and that this net migration of grana membrane proteins resulted in a 23% decrease in the amount of stacked membranes. Both of these phenomena were reversed following dephosphorylation of the LHCII complexes. Throughout these events, the basic 3D architecture of the thylakoids remained unchanged except for the change in the amount of membrane stacking (see figures 2 and 3B in Kyle et al., 1983), suggesting that the changes in membrane stacking are brought about by simple membrane flow between grana and stroma thylakoids.

These results contradict the hypothetical model of state I/II-induced thylakoid membrane changes recently proposed by Chuartzman et al. (2008). Their hypothetical model is based on the controversial bifurcated thylakoid membrane model of Shimoni et al. (2005), and postulates that during state I → state II

transitions entire stacked membrane domains become separated and that some of the membrane bridges between such grana thylakoids are ruptured during the unstacking process. These ruptured membrane bridges are postulated to be reformed when the LHCII molecules are dephosphorylated and the membranes restack. During the course of our very extensive analyses of the effects of state I/II transitions on thylakoid organization by means of freeze-fracture electron microscopy (Kyle et al., 1983), we never observed any evidence for ruptured thylakoids.

MATERIALS AND METHODS

Plant Material

Seeds of Arabidopsis (*Arabidopsis thaliana*; Landsberg *erecta*) and tobacco (*Nicotiana tobacum*) were planted on 0.8% (w/v) agar plates with Murashige and Skoog medium and 1% Suc for 5 d. Plants were grown at a temperature of 23°C, light intensity of 150 mmol μm^{-2} s^{-1}, and a photoperiod of 16/8 light/dark. Fresh spinach (*Spinacia oleracea*) was bought at a local supermarket (Whole Food Market) and used the same day.

Intact Chloroplast Isolation

Fifty grams of washed spinach leaves were added to 125 mL of buffer 1 (0.4 M NaCl, 2 mM MgCl, 0.2% bovine serum albumin, and 20 mM Tricine, pH 8.0) and diced in a blender equipped with razor blades. This was filtered through four layers of cheesecloth, and centrifuged at 300*g* for 1 min. The supernatant was centrifuged at 4,000g to pellet the chloroplasts. The resulting chloroplast pellet was gently washed with buffer 2 (0.15 M NaCl, 5 mM MgCl, 0.2% bovine serum albumin, and 20 mM Tricine, pH 8.0) without disruption of the chloroplasts. The supernatant was removed and replaced with buffer 3 (0.4 M Suc, 0.15 mM NaCl, 5 mM MgCl, and 20 mM HEPES, pH 7.5).

Sample Preparation for Electron Tomography

Leaves were removed from plants and transferred to aluminum sample holders and cryoprotected with 150 mM Suc, or freshly isolated chloroplasts were placed into an aluminum holder, and frozen in a Baltec HPM 010 high-pressure freezer (RMC). Samples were then freeze substituted in 2% OsO_4 in anhydrous acetone at −80°C for 5 d. The samples were warmed to −20°C and washed with −20°C anhydrous acetone, followed by slow warming to room temperature over a period of 24 h. The samples were removed from their holders and infiltrated with increasing concentrations of EPON resin (Ted Pella). Polymerization was performed at 60°C for 24 h. EPON sections 80 to 350 nm were placed on Formvar (Ted Pella) copper slot grids for electron microscopy. To prepare grids for electron tomographic data collection, 10 μL of 15 nm colloidal gold was precipitated onto grids containing thick sections for 10 min on each side.

Intermediate- and High-Voltage Electron Microscopy and Acquisition of Tilt Series Images

Seventeen tomograms were collected on a Tecnai TF30 (FEI) intermediate voltage electron microscope operating at 300 kV. The images were taken at 20,000× from +60 to −60 at 1° intervals about two orthogonal axes (Ladinsky et al., 1997), and collected with a Gtan Megascan 795 digital camera that covered an area of 2.6 × 2.6 mm^2 and had a resolution of 2,048 × 2,048 pixels at a pixel size of 1.26 nm. The remaining tomograms were collected on a JEM-1000 high-voltage electron microscope (JEOL) operating at 750 kV. The images were collected as described by Austin et al. (2005).

3D Tomographic Reconstruction, Modeling, and Analysis

The images (single or montaged frames) were aligned using the gold particles as fiducial markers as described previously (Ladinsky et al., 1999). Each set of aligned tilts was reconstructed into a single-axis tomogram using the R-weighted back-projection algorithm (Gilbert, 1972). Merging the two single-axis tomograms into a dual-axis tomogram involved a warping procedure rather than a single linear transformation to produce the dual-axis tomogram (Mastronarde, 1997). In addition, dual-axis tomograms computed from adjacent serial sections were aligned and joined to increase the reconstructed volume (Austin et al., 2005). Tomograms were displayed and analyzed with 3dmod, the graphics component of the 3DMOD (formerly IMOD) software package (Kremer et al., 1996). Membranous structures, microtubules, and all types of vesicles were modeled as described previously (Otegui and Austin, 2007). Once a model was completed, meshes of triangles were computed to define the surface of each object (Kremer et al., 1996).

The image-slicer tool of 3DMOD was used to display and analyze tomographic slices extracted from the tomogram in any position or tilt around the *x*, *y*, or *z* axis. This tool allowed us to obtain squeezed images in which a number of consecutive 2.2-nm tomographic slices were combined, thus generating *z* projections of different thicknesses, more similar to conventional electron microscopy thin sections.

Supplemental Data

The following materials are available in the online version of this article.

Supplemental Figure S1. Three-dimensional model illustrating the spatial relationship between stacked grana and interconnecting stroma thylakoids based on an electron tomography analysis of high pressure frozen and freeze-substituted intact chloroplasts.

Supplemental Video S1. Tomographic volume of a complete grana thylakoid stack and associated interconnected stroma thylakoids.

ACKNOWLEDGMENTS

We would like to thank Katie Lundeen for her assistance in preparing samples for electron microscopy, and David Mastronarde and Richard Gaudette for providing essential application software and support.

Received December 6, 2010; accepted December 24, 2010; published January 11, 2011.

LITERATURE CITED

Allen JF (1992) Protein phosphorylation in regulation of photosynthesis. Biochim Biophys Acta **1098:** 275–335

Anderson JM (1999) Insights into the consequences of grana stacking of thylakoid membranes in vascular plants: a personal perspective. Aust J Plant Physiol **26:** 625–639

Anderson JM, Andersson B (1988) The dynamic photosynthetic membrane and regulation of solar energy conversion. Trends Biochem Sci **13:** 351–355

Anderson JM, Goodchild DJ, Boardman NK (1973) Composition of the photosystems and chloroplast structure in extreme shade plants. Biochim Biophys Acta **325:** 573–585

Andersson B, Anderson JM (1980) Lateral heterogeneity in the distribution of chlorophyll-protein complexes of the thylakoid membranes of spinach chloroplasts. Biochim Biophys Acta **593:** 427–440

Aro EM, Suorsa M, Rokka A, Allahverdiyeva Y, Paakkarinen V, Saleem A, Battchikova A, Rintamäki E (2004) Dynamics of photosystem II: a proteomic approach to thylakoid protein complexes. J Exp Bot **56:** 347–356

Arvidsson PO, Sundby C (1999) A model for the topology of the chloroplast thylakoid membrane. Aust J Plant Physiol **26:** 687–694

Austin JR II, Seguí-Simarro JM, Staehelin LA (2005) Quantitative analysis of changes in spatial distribution and plus-end geometry of microtubules involved in plant-cell cytokinesis. J Cell Sci **118:** 3895–3903

Barber J (1982) Influence of surface charges on thylakoid structure and function. Annu Rev Plant Physiol **33:** 261–295

Bassi R, dal Belin Peruffo A, Barbato R, Ghisi R (1985) Differences in chlorophyll-protein complexes and composition of polypeptides between thylakoids from bundle sheaths and mesophyll cells in maize. Eur J Biochem **146:** 589–595

Brangeon J (1974) Structural modifications in the lamellar system of

isolated *Zea mays* chloroplasts under different ionic conditions. J Microsc **21:** 75–84

Brangeon J, Mustárdy L (1979) The ontogenic assembly of intra-chloroplast lamellae viewed in 3-dimensions. Biol Cell **36:** 71–80

Briantais JM (1984) Kinetics of cation-induced changes of photosystem II fluorescence and of lateral distribution of the two photosystems in the thylakoid membrane of pea thylakoids. Biochim Biophys Acta **766:** 1–8

Chuartzman SG, Nevo R, Shimoni E, Charuvi D, Kiss V, Ohad I, Brumfeld V, Reich Z (2008) Thylakoid membrane remodeling during state transitions in *Arabidopsis*. Plant Cell **20:** 1029–1039

Daum B, Nicastro D, Austin J II, McIntosh JR, Kühlbrandt W (2010) Arrangement of photosystem II and ATP synthase in chloroplast membranes of spinach and pea. Plant Cell **22:** 1299–1312

Dekker JP, Boekema EJ (2005) Supramolecular organization of thylakoid membrane proteins in green plants. Biochim Biophys Acta **1706:** 12–39

Donohoe BS, Mogelsvang S, Staehelin LA (2006) Electron tomography of ER, Golgi and related membrane systems. Methods **39:** 154–162

Giddings TH, Withers NW, Staehelin LA (1980) Supramolecular structure of stacked and unstacked regions of the photosynthetic membranes of Prochloron sp., a prokaryote. Proc Natl Acad Sci USA **77:** 352–356

Gilbert PF (1972) The reconstruction of a three-dimensional structure from projections and its application to electron microscopy: II. Direct methods. Proc R Soc Lond B Biol Sci **182:** 89–102

Gilkey JC, Staehelin LA (1986) Advances in ultrarapid freezing for the preservation of cellular ultrastructure. J Electron Microsc Tech **3:** 177–210

Goodenough UW, Staehelin LA (1971) Structural differentiation of stacked and unstacked chloroplast membranes: freeze-etch electron microscopy of wild-type and mutant strains of Chlamydomonas. J Cell Biol **48:** 594–619

Heslop-Harrison J (1963) Structure and morphogenesis of lamellar systems in grana-containing chloroplast. I. Membrane structure and lamellar architecture. Planta **60:** 243–260

Hodge AJ, McLean JD, Mercer FV (1955) Ultrastructure of the lamellae and grana in the chloroplast of Zea mays L. J Biophys Biochem Cytol **25:** 605–614

Izawa S, Good NE (1966) Effects of salts and electron transport on the conformation of isolated chloroplasts. II. Electron microscopy. Plant Physiol **41:** 544–552

Kirchhoff H, Haase W, Haferkamp S, Schott T, Borinski M, Kubitscheck U, Rögner M (2007) Structural and functional self-organization of Photosystem II in grana thylakoids. Biochim Biophys Acta **1767:** 1180–1188

Kiss JZ, Staehelin LA (1995) High pressure freezing. *In* NJ Severs, DM Shotton, eds, Rapid Freezing, Freeze Fracture and Deep Etching. John Wiley-Liss Inc., New York, pp 89–104

Kremer JR, Mastronarde DN, McIntosh JR (1996) Computer visualization of three-dimensional image data using IMOD. J Struct Biol **116:** 71–76

Król M, Spangfort MD, Huner NP, Oquist G, Gustafsson P, Jansson S (1995) Chlorophyll a/b-binding proteins, pigment conversions, and early light-induced proteins in a chlorophyll b-less barley mutant. Plant Physiol **107:** 873–883

Kyle DJ, Staehelin LA, Arntzen CJ (1983) Lateral mobility of the light-harvesting complex in chloroplast membranes controls excitation energy distribution in higher plants. Arch Biochem Biophys **222:** 527–541

Ladinsky MS, Kremer JR, Mastronarde DN, McIntosh JR, Staehelin LA, Howell KE (1997) HVEM tomography of the Golgi ribbon in cryofixed NRK cells: the non-compact region, the CGN, and TGN. Mol Biol Cell **8:** 2040

Ladinsky MS, Mastronarde DN, McIntosh JR, Howell KE, Staehelin LA (1999) Golgi structure in three dimensions: functional insights from the normal rat kidney cell. J Cell Biol **144:** 1135–1149

Mastronarde DN (1997) Dual-axis tomography: an approach with alignment methods that preserve resolution. J Struct Biol **120:** 343–352

McDonnel A, Staehelin LA (1980) Adhesion between liposomes mediated by the chlorophyll a/b light-harvesting complex isolated from chloroplast membranes. J Cell Biol **84:** 40–56

McIntosh R, Nicastro D, Mastronarde D (2005) New views of cells in 3D: an introduction to electron tomography. Trends Cell Biol **15:** 43–51

Menke W (1960) Das allgemeine Bauprinzip des Lamellarsystems der Chloroplasten. Experientia **16:** 537–538

Menke W (1962) Structure and chemistry of plastids. Annu Rev Plant Physiol **13:** 27–44

Miller KR, Staehelin LA (1973) Fine Structure of the chloroplast membranes of Euglena gracilia as revealed by freeze-cleaving and deep-etching techniques. Protoplasma **7:** 55–78

Miller KR, Staehelin LA (1976) Analysis of the thylakoid outer surface. J Cell Biol **68:** 30–47

Mullineaux CW (2005) Function and evolution of grana. Trends Plant Sci **10:** 521–525

Mustárdy L, Buttle K, Steinbach G, Garab G (2008) The three-dimensional network of the thylakoid membranes in plants: quasihelical model of the granum-stroma assembly. Plant Cell **20:** 2552–2557

Mustárdy L, Garab G (2003) Granum revisited: a three-dimensional model—where things fall into place. Trends Plant Sci **8:** 117–122

Mustárdy L, Jánossy AGS (1979) Evidence of helical thylakoid arrangement by scanning electron microscopy. Plant Sci Lett **16:** 281–284

Otegui MS, Austin JR II (2007) Visualization of membrane-cytoskeletal interactions during plant cytokinesis. Methods Cell Biol **79:** 221–240

Paolillo DJ Jr (1970) The three-dimensional arrangement of intergranal lamellae in chloroplasts. J Cell Sci **6:** 243–255

Paolillo DJ Jr, Falk RH, Reighard JA (1967) The effect of chemical fixation on the fretwork of chloroplasts. Trans Am Microsc Soc **86:** 225–232

Shimoni E, Rav-Hon O, Ohad I, Brumfeld V, Reich Z (2005) Three-dimensional organization of higher-plant chloroplast thylakoid membranes revealed by electron tomography. Plant Cell **17:** 2580–2586

Staehelin LA (1976) Reversible particle movements associated with unstacking and restacking of chloroplast membranes in vitro. J Cell Biol **71:** 136–158

Staehelin LA (1986) Photosynthesis III: Photosynthetic Membranes. *In* CJ Arntzen, LA Staehelin, eds, Springer-Verlag, Berlin, pp 1–84

Staehelin LA (2003) Chloroplast structure: from chlorophyll granules to supra-molecular architecture of thylakoid membranes. Photosynth Res **76:** 185–196

Staehelin LA, Armond PA, Miller KR (1977) Chloroplast membrane organization at the supramolecular levels and its functional implications. Brookhaven Symp Biol **28:** 278–315

Staehelin LA, Arntzen CJ (1983) Regulation of chloroplast membrane function: protein phosphorylation changes the spatial organization of membrane components. J Cell Biol **97:** 1327–1337

Staehelin LA, van der Staay GWM (1996) Structure, composition, functional organisation and dynamic properties of thylakoid membranes. *In* DR Ort, CF Yocum, eds, Oxygenic Photosynthesis: The Light Reactions. Kluwer Academic Publishers, Dordrecht, The Netherlands, pp 11–30

Steinmann E, Sjöstrand FS (1955) The ultrastructure of chloroplasts. Exp Cell Res **8:** 15–23

Trissl HW, Wilhelm C (1993) Why do thylakoid membranes from higher plants form grana stacks? Trends Biochem Sci **18:** 415–419

Varga AR, Staehelin LA (1983) Spatial differentiation in photosynthetic and non-photosynthetic membranes of Rhodopseudomonas palustris. J Bacteriol **154:** 1414–1430

Wehrmeyer W (1964) Zur klärung der structurellen variabilität der chloroplastengrana des spinats in profil und aufsicht. Planta **62:** 272–293

Weier TE (1961) The ultramicrostructure of starch free chloroplasts of Nicotiana rustica. Am J Bot **48:** 615–630

Weier TE, Stocking CR, Thomoson WW, Drever H (1963) The photosynthetic apparatus in chloroplast of higher plants. J Ultrastruct Res **8:** 122–143